Cancer Research

# α3β1 Integrin Suppresses Prostate Cancer Metastasis via Regulation of the Hippo Pathway

Afshin Varzavand[1], Will Hacker[2], Deqin Ma[3], Katherine Gibson-Corley[3], Maria Hawayek[1], Omar J. Tayh[1], James A. Brown[4], Michael D. Henry[3,5], and Christopher S. Stipp[1,5]

## Abstract

Existing anticancer strategies focused on disrupting integrin functions in tumor cells or tumor-involved endothelial cells have met limited success. An alternative strategy is to augment integrin-mediated pathways that suppress tumor progression, but how integrins can signal to restrain malignant behavior remains unclear. To address this issue, we generated an *in vivo* model of prostate cancer metastasis via depletion of α3β1 integrin, a correlation observed in a significant proportion of prostate cancers. Our data describe a mechanism whereby α3β1 signals through Abl family kinases to restrain Rho GTPase activity, support Hippo pathway suppressor functions, and restrain prostate cancer migration, invasion, and anchorage-independent growth. This α3β1-Abl kinase-Hippo suppressor pathway identified α3 integrin–deficient prostate cancers as potential candidates for Hippo-targeted therapies currently under development, suggesting new strategies for targeting metastatic prostate cancer based on integrin expression. Our data also revealed paradoxical tumor suppressor functions for Abl kinases in prostate cancer that may help to explain the failure of Abl kinase inhibitor imatinib in prostate cancer clinical trials. *Cancer Res; 76(22); 6577–87. ©2016 AACR.*

## Introduction

Changes in cell–extracellular matrix interactions are hallmarks of prostate cancer progression (1, 2), yet our understanding of the mechanistic contributions of these events is far from complete. For example, altered integrin expression has been noted in prostate cancer (1, 2); however, translating knowledge of changes in integrin expression and function into the clinical setting has proved challenging. Thus far, αv integrin–targeting agents have been tested clinically in prostate cancer, and multiple trials using an anti-αv antibody, or ligand-mimetic peptide failed to show clinical benefit (3–5). Existing integrin-directed therapeutic strategies disrupt integrin function, but integrins can also exert tumor-suppressive activities (6–8). Therefore, an alternative yet neglected approach would be to augment integrin-mediated tumor suppressor functions. In prostate cancer, reduced α3 integrin expression was suggested to associate with a more aggressive phenotype (9), but whether α3 downregulation contributes mechanistically to prostate cancer progression was unknown. Our recent study revealed that loss of α3 integrin can indeed promote prostate cancer colonization of metastatic sites (10), but did not identify the signaling mechanism by which α3 integrin restrains malignant behavior or whether α3 functions at earlier stages in prostate cancer progression.

The Hippo tumor suppressor pathway is a master integrator of multiple extracellular inputs, including cell adhesion and detachment, cell–cell contacts, and growth factor signaling (11–13). Although the Hippo pathway is clearly influenced by cell adhesion, aside from E-cadherin, few specific adhesion receptors have been identified as upstream inputs. We now provide evidence of an α3 integrin-Abl kinase-Hippo suppressor pathway in prostate cancer in which α3β1 integrin signals through Abl kinases to restrain Rho GTPase activity, sustain Hippo suppressor functions, and curtail metastatic cell phenotypes. Importantly, multiple members of this novel α3-Abl-Hippo pathway are amenable to pharmacologic manipulation, suggesting new strategies for targeting metastatic prostate cancer based on integrin expression.

## Materials and Methods

### Cell culture

GS6889.Li cells, a metastatic subline of PC-3 prostate carcinoma cells created in 2009 (14), were reauthenticated in 2016 for this study by STR analysis (IDEXX Bioresearch). DU-145 prostate carcinoma cells, originally obtained from ATCC in 2005, were cultured for fewer than 20 additional passages from the original stock during the course of the present study. GS689.Li cells and DU-145 cells were cultured in DMEM:F12 with 10% FBS. Cells were transduced with a pQCXIN retroviral expression vector encoding luciferase, and a pQCXIP retroviral vector encoding GFP.

### Antibodies and reagents

Antibodies used were: α3 integrin, A3-X8 (8); A3-CYT (15); and HPA008572, (Sigma-Aldrich); RhoA (ARHO1, Cytoskeleton Inc); RhoC, (D40E4, Cell Signaling Technology); actin (AC-15, Sigma-

[1]Department of Biology, Holden Comprehensive Cancer Center, University of Iowa, Iowa City, Iowa. [2]Department of Biochemistry, Holden Comprehensive Cancer Center, University of Iowa, Iowa City, Iowa. [3]Department of Pathology, Holden Comprehensive Cancer Center, University of Iowa, Iowa City, Iowa. [4]Department of Urology, Holden Comprehensive Cancer Center, University of Iowa, Iowa City, Iowa. [5]Department of Molecular Physiology and Biophysics, Holden Comprehensive Cancer Center, University of Iowa, Iowa City, Iowa.

**Note:** Supplementary data for this article are available at Cancer Research Online (http://cancerres.aacrjournals.org/).

Current address for M. Hawayek: University of Puerto Rico, San Juan, Puerto Rico.

**Corresponding Author:** Christopher S. Stipp, University of Iowa, 210 E. Iowa Ave., BBE 236, Iowa City, IA, 52242. Phone: 319-335-0192; Fax: 319-335-1069; E-mail: christopher-stipp@uiowa.edu

**doi:** 10.1158/0008-5472.CAN-16-1483

Aldrich); LATS1 C66B5, YAP/TAZ D24E4 (Cell Signaling Technology); TAZ/WWTR1 (1H9, Lifespan Biosciences, Inc); YAP1 (H-125, Santa Cruz Biotechnology); CTGF (L-20, Santa Cruz Biotechnology); β-catenin (610153, BD Biosciences); p190RhoGAP (D2D6, Millipore); phosphotyrosine (P-Tyr-100, Cell Signaling Technology); p120RasGAP (B4F8, Santa Cruz Biotechnology); Crk (22/Crk, BD Biosciences); phospho-Crk/CrkL, (#3181, Cell Signaling Technology); Arg/Abl2 (A301-986A, Bethyl Laboratories, Inc); and FAK and phospho-FAK (77/FAK and 18/FAK (pY397; BD Biosciences). Secondary reagents were PE-goat anti-mouse, Alexa 680 goat anti-mouse, Alexa 790 goat anti-rabbit, and Dylight 800 Neutravidin (Thermo Fisher Scientific).

Other reagents were D-luciferin (Gold Biotechnology), rat tail collagen I (Corning), C3 transferase (Cytoskeleton, Inc), lysophasphatidic acid (LPA; Avanti Polar Lipids), Y-27632 (Enzo Life Sciences), blebbistain (Selleckchem), imatinib (Cayman Chemical), DPH [5-(1,3-diaryl-1H-pyrazol-4-yl) hydantoin, 5-[3-(4-fluorophenyl)-1-phenyl-1H-pyrazol-4-yl]-2,4-imidazolidinedione] (Sigma-Aldrich), and PF-573228 (Tocris).

### RNA interference

α3-KD, LATS sh1-sh4, shYAP, shTAZ, YAP sh1, YAP sh2, and Arg retroviral shRNA constructs had a pSIREN RetroQ vector backbone (Clontech); α3-KD2, TAZ sh1-sh3, and Abl sh1-sh3 constructs had a pZIP-mCMV-ZsGreen backbone (Transomics Technologies). RhoA, RhoC and LATS sh5 and sh6 constructs had a pLKO backbone (Sigma-Aldrich). A nontargeting shRNA in the appropriate vector backbone was included to produce vector control cell lines. Cells were maintained as stably transduced, polyclonal populations. For details, see Supplementary Information or RNAi targeting sequences.

### Orthotopic prostate cancer models

Animal protocols were approved by the University of Iowa Animal Care and Use Committee (Approval #5031328). GS689.Li cells ($5 \times 10^4$) were implanted in the left anterior lobe of the prostate of 8 SCID/NCr (BALB/C) mice/cell line. Bioluminescent imaging (BLI) was performed using an Ami X imaging system (Spectral Instruments Imaging) as described previously (10). Upon sacrifice, livers, kidneys, and lungs were dissected for analysis of disseminated cells by fluorescence microscopy. Liver and kidney colonization was imaged with an Olympus SZX12 stereomicroscope. To image lung metastases, one lobe of each lung was cut into approximately 3–5 mm pieces and flattened between two glass slides. Ten random fields per lung were photographed using the 10× objective of a Leica DMIRE2 inverted microscope. Areas occupied by GFP-labeled cells were determined using the ImageJ Threshold command followed by the Analyze Particle command (size range 50.00-Infinity $\mu m^2$). A similar approach was used to quantify kidney and liver colonization except that the data were converted to %GFP-positive area by dividing by the total area of each kidney or liver. Anterior and posterior aspects of each liver and dorsal and ventral aspects of each kidney were examined.

### *In vitro* tumor growth assays

***3D collagen growth assay.*** Collagen I (300 μL; 0.8 mg/mL in DMEM) was polymerized per well in 24-well plates for 45 minutes at 37°C. A total of $1.5 \times 10^4$ cells per well were seeded in 500 μL of defined growth medium [DGM; DMEM: F12, 5 mg/mL BSA, 2 mmol/L L-glutamine, 100 U/mL penicillin, 100 μg/mL streptomycin, 0.1 mmol/L nonessential amino acids, 25 mmol/L HEPES pH 7.2, plus insulin–transferrin–selenium (ITS) supplement]. After 7–10 days, cell number was quantified by BLI. Six wells/cell type/condition were quantified in each trial.

***Detached growth assay.*** Twenty-four–well plates were treated twice with 100 μL/well of 20 mg/mL poly-HEMA [Poly(2-hydroxyethyl methacrylate)] in 95% ethanol, which was allowed to evaporate. Wells were rinsed with PBS and $1.5 \times 10^4$ cells were seeded per well in 500 μL of DGM. After 7–10 days, cell growth was quantified by BLI.

***Starvation growth assay.*** A total of $1.5 \times 10^4$ cells per well were plated in uncoated 24-well plates in serum-free medium (SFM; DMEM:F12, 5 mg/mL BSA, 2 mmol/L L-glutamine, 100 U/mL penicillin, 100 μg/mL streptomycin, and 0.1 mmol/L nonessential amino acids, 25 mmol/L HEPES pH 7.2, no ITS supplement). After 7–10 days, cell growth was quantified by BLI.

### Time-lapse microscopy and transwell migration assays

A total of $2.3 \times 10^5$ cells were plated in SFM on 35-mm dishes coated with 10 μg/mL rat tail collagen I. Time-lapse images were acquired as described previously (15). ImageJ software was used to record the XY position of 50–70 cell centroids in frames 5 minutes apart and determine the migration speed, using the mTrackJ plugin (16). In the cell contraction assay, serum-starved cells were stimulated with 10% FBS, and cell areas were measured in frames 1 minute apart using ImageJ.

For Matrigel invasion, $2.5 \times 10^4$ cells per well were seeded in SFM in the top wells of BD BioCoat Matrigel invasion chambers. SFM with 5 μmol/L LPA was placed in the lower well. After 24 hours, cells were stained with Cell Tracker Red (ThermoFisher Scientific), and noninvaded cells were removed using a cotton swab. Invaded cells were quantified in 4 fields per chamber representing peripheral and central parts of the chamber.

### Rho activity assays

Confluent 100-mm dishes were serum-starved overnight and stimulated with 5 μmol/L LPA for indicated amounts of time. Cells were lysed with ice-cold 1% Triton X-100, 0.1% SDS, 10 mmol/L $MgCl_2$ with protease inhibitors, and activated Rho was recovered by pulldown with GST-Rhotekin fusion protein, followed by immunoblotting for active and total Rho, as described previously (17).

### Immunoblotting and immunoprecipitation

Immunoprecipitations and blotting were performed as described previously (15) and quantified using a LiCOR Odyssey blot imager. For immunoprecipitation of p190RhoGAP complexes, cell lysates were prepared in 1% Triton X-100 detergent. For analysis of YAP and TAZ protein in cells growing under detached conditions, cells were grown in DGM in suspension over poly-HEMA for 4–11 days prior to lysis.

### Immunohistochemistry

Antigen unmasking was in citrate buffer, pH 6. Endogenous peroxidase was quenched with 3% $H_2O_2$, and either 1.5% horse

serum (α3 integrin) or 10% goat serum (TAZ and YAP) was used to block nonspecific staining. Sections were incubated with rabbit anti-α3 integrin (HPA008572) at 1:20, mouse anti-WWTR1/TAZ (1H9) at 1:100 or rabbit anti-YAP (Santa Cruz Biotechnology sc-15407) at 1:100 for 1 hour. Slides were incubated with secondary antibody and detection reagent (DAKO Rabbit Envision HRP

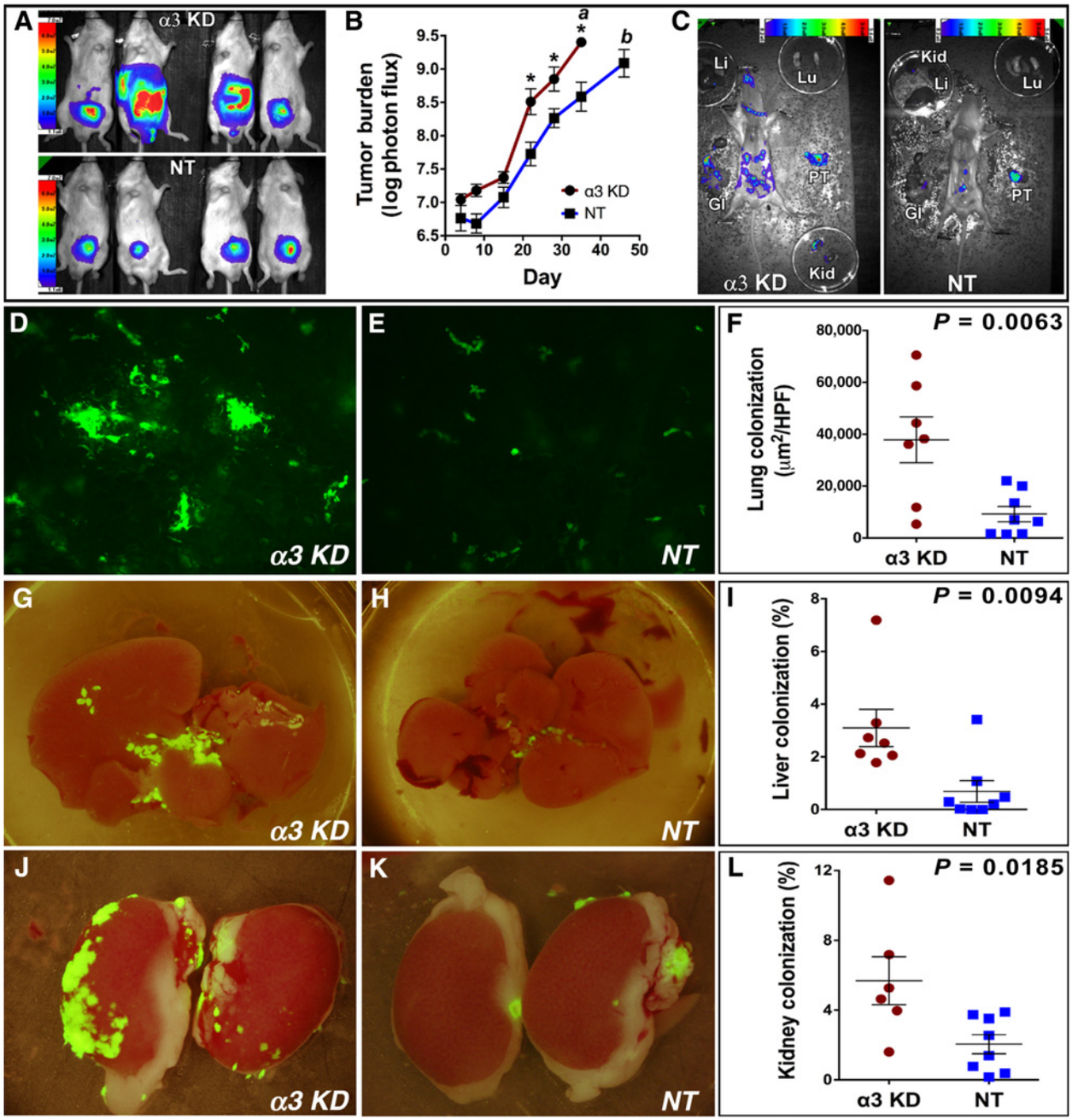


**Figure 1.**

Loss of α3 integrin promotes prostate cancer progression and metastasis *in vivo*. **A,** bioluminescence imaging of orthotopic tumors 28 days postimplantation. Color scale indicates photons/sec/cm$^2$/sr. **B,** tumor burden versus time. **a,** mice harboring α3-KD tumors and one mouse harboring an NT control tumor were sacrificed on day 35. **b,** the remaining mice harboring NT control tumors were sacrificed on day 46. *, $P = 0.0004$; $P = 0.007$; and $P = 0.001$ on days 21, 28, and 35, respectively, Holm–Sidak multiple comparison test with $\alpha = 0.05$. **C,** gross necropsies of mice harboring α3-KD and NT control tumors on day 35. Tumor burden of both mice was approximately $1 \times 10^9$ photons/sec. PT, primary tumor; GI, gastrointestinal tract; Kid, kidney; Li, liver; Lu, lung. **D** and **E,** representative images of GFP-labeled α3-KD and NT control lung metastases. **F,** quantification of lung metastasis as μm$^2$ GFP-positive cells per high-powered field (HPF). $P = 0.0063$, unpaired *t* test. **G** and **H,** liver colonization by GFP-labeled α3-KD and NT control cells. **I,** quantification of liver colonization as percentage of total surface area occupied by tumor cells. $P = 0.0094$, unpaired *t* test. **J** and **K,** kidney colonization by GFP-labeled α3-KD and NT control cells. **L,** quantification of kidney colonization as percentage of total surface area occupied by tumor cells. $P = 0.0185$, unpaired *t* test.

System reagent for 30 minutes for α3 integrin and YAP, and biotinylated anti-mouse IgG at 1:500 followed by ABC for TAZ). Slides were developed with DAKO DAB plus for 5 minutes, DAB Enhancer for 3 minutes, and counterstained with hematoxylin.

***Quartile staining system.*** For α3 integrin, 3 = strong basal staining typical of benign glands; 2 = reduced, delocalized staining; 1 = faint, discontinuous staining; and 0 = essentially absent staining. For TAZ, 3 = most nuclei show strong staining, clearly higher than cytoplasmic staining; 2 = moderate staining, majority of nuclei still clearly positive; 1 = faint staining, many nuclei appear negative; 0 = absence of nuclear staining characteristic of the luminal cells of most benign glands (note that proliferative basal cells in benign glands are TAZ positive). For YAP, 3 = most nuclei show strong staining, clearly higher than cytoplasmic staining; 2 = intermediate staining, some nuclei appear more highly stained than adjacent cytoplasm; 1 = faint staining, a few scattered nuclei appear more highly stained than adjacent cytoplasm; 0 = faint cytoplasmic staining, unstained nuclei characteristic of luminal cells of benign glands.

## Results

### Loss of α3 integrin promotes prostate cancer progression and metastasis and growth under low-anchorage and low growth factor conditions

To investigate the contribution of α3 integrin to prostate cancer progression and spontaneous metastasis, we inoculated luciferase and GFP-labeled α3-depleted (α3-KD) and vector control (NT) cells in the left anterior lobe of the mouse prostate. At 28 days postinoculation, mice harboring α3-KD cells showed dramatically increased apparent tumor burdens by BLI (Fig. 1A). The α3-KD cells showed significantly higher BLI signal from day 22 to day 35, at which time the mice harboring α3-KD cells had reached a predefined BLI endpoint of $>10^9$ photons/second total tumor burden (Fig. 1B, annotation "a"). Flow cytometry confirmed that α3 integrin was approximately 90% depleted in the α3-KD cells (Supplementary Fig. S1), as reported previously (10).

On day 35, the mouse with the highest burden of NT control cells was sacrificed along with the mice harboring the α3-KD cells. This NT control mouse was compared with an α3-KD mouse with a similar total tumor burden. A BLI-assisted gross necropsy revealed widespread dissemination of α3-KD cells compared with NT cells (Fig. 1C). Therefore, we allowed the remainder of the mice harboring NT cells to continue for another 11 days, until their mean BLI signal approached that of the α3-KD cell mice on day 35 (Fig. 1B, annotation b). We took this approach to account for the possibility that increased dissemination was simply a function of increased α3-KD tumor growth. Disseminated α3-KD and NT cells were imaged by GFP fluorescence in tissues harvested just after sacrifice on day 35 and day 46, respectively. Compared with the NT cells, the α3-KD cells showed increased lung metastasis (Fig. 1D–F), and increased liver and kidney colonization (Fig. 1G–L). The primary tumor burden of α3-KD tumors and NT tumors was not significantly different at the time of sacrifice (Supplementary Fig. S2A). Nevertheless, we normalized the lung, liver, and kidney data to the primary tumor BLI just prior to sacrifice. Even after adjusting for primary tumor signal, α3-KD cells showed greater lung metastasis and liver colonization (Supplementary Fig. S2B and S2C), and an increased trend of kidney colonization (Supplementary Fig. S2D), suggesting that the loss of α3 integrin promotes dissemination from the prostate in addition to more rapid primary tumor growth.

We identified multiple *in vitro* assays of tumor cell growth that recapitulated the increased growth of the α3-KD tumors *in vivo*. Culturing cells on 3D collagen, under detached conditions, or under serum starvation all uncovered dramatically increased growth of α3-KD cells (Fig. 2A–C and Supplementary Fig. S3A

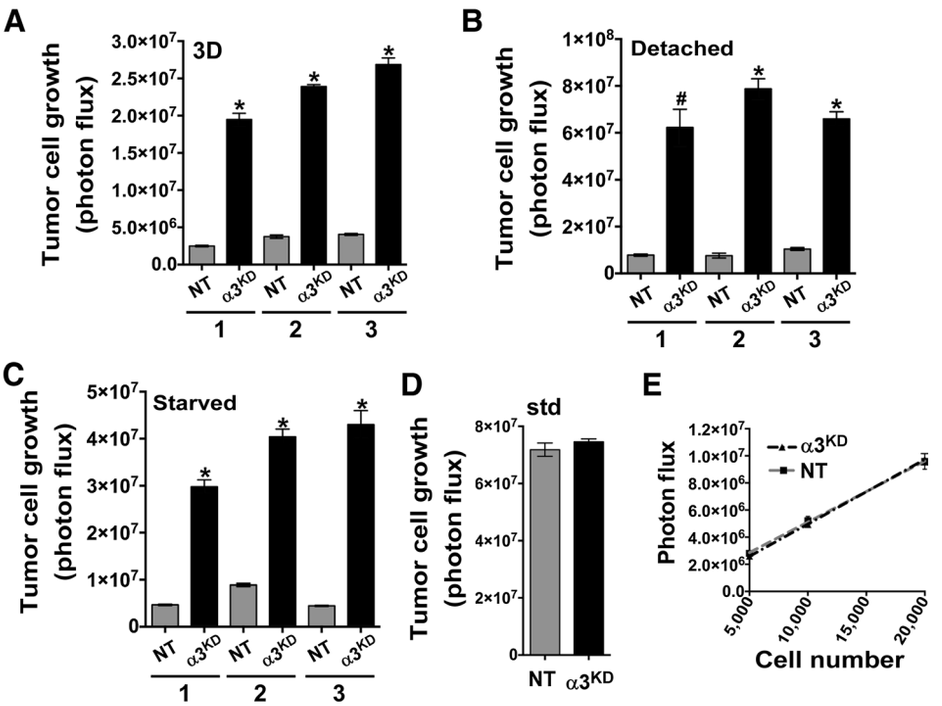


**Figure 2.**
Loss of α3 integrin promotes growth under low-anchorage and low growth factor conditions. Tumor cell growth (**A**) on a 3D collagen matrix, under detached conditions (**B**), floating over a poly-HEMA coated surface, and on a 2D matrix under serum growth factor deprivation is shown for three independent trials of each condition (**C**). *, $P < 0.0001$, #, $P = 0.0022$, unpaired $t$ test. **D,** tumor cell growth under standard tissue culture conditions in 10% FBS. **E,** both α3-KD and NT control cells have a similar photon flux/cell and are not significantly different, $P = 0.5512$, linear regression analysis. Error bars, ± SEM, $n = 6$ wells per cell type/number of cells.

and S3B). Importantly, growth of the cells under standard 2D culture conditions in 10% serum did not reveal any difference (Fig. 2D); thus, the growth advantage of α3-KD cells pertains to low anchorage and/or low growth factor conditions. Control experiments confirmed that α3-KD and NT cells have virtually identical luminescence (Fig. 2E), eliminating the trivial possibility that differences between α3-KD and NT control cells *in vivo* and *in vitro* are due to BLI intensities. Silencing α3 integrin in another prostate cancer cell line, DU-145, produced similar results (Supplementary Fig. S3C and S3D).

### The increased growth of α3-KD cells is linked to aberrant RhoA signaling

Genetic deletion of α3 integrin causes aberrant signaling through Rho GTPases in both mammary myoepithelial cells and neurons (18, 19). Therefore, we investigated the kinetics of Rho activation in α3-KD and NT cells. In α3-KD cells, LPA stimulation triggered a prolonged activation of both RhoA and RhoC. In contrast, Rho activation was more transient in NT cells, returning to baseline by 30 minutes poststimulation (Fig. 3A and B).

As Rho signaling can promote anchorage-independent growth (20), we examined the effect on 3D growth of inhibiting Rho with C3 transferase or activating Rho with LPA. C3 transferase strongly suppressed the increased growth of the α3-KD cells (Fig. 3C), while LPA promoted 3D growth of both NT and α3-KD cells, and maximal Rho stimulation abolished the growth difference between the two cell types (Fig. 3D). This was consistent with α3 integrin functioning upstream to limit Rho-dependent 3D growth, with maximal Rho activation overriding α3's suppressor effects.

We next used retroviral RNAi to silence RhoA or RhoC in α3-KD cells. RhoC was upregulated in the RhoA knockdown cells, while RhoA was upregulated in the RhoC knockdown cells, consistent with an earlier report (Fig. 3E; ref. 21). Strikingly, depleting RhoA significantly blocked the 3D growth of α3-KD cells (Fig. 3F), but depleting RhoC actually increased 3D growth, to an extent that correlated with the extent of RhoA upregulation observed in the RhoC knockdown cells in Fig. 3E. An additional shRNA that produced strong RhoA knockdown also strongly suppressed the increased growth of α3-KD cells in 3D collagen and detached conditions (Fig. 3G and H).

Rho-driven anchorage-independent growth is linked to increased myosin-driven contractility (20). Indeed, we found that α3-KD cells displayed a hypercontractile phenotype upon serum stimulation (Supplementary Fig. S4A and S4B), and the myosin inhibitor blebbistain dramatically reduced the growth of α3-KD cells under low growth factor or low anchorage conditions, with no effect on the low basal growth of NT control cells (Supplementary Fig. S4C and S4D).

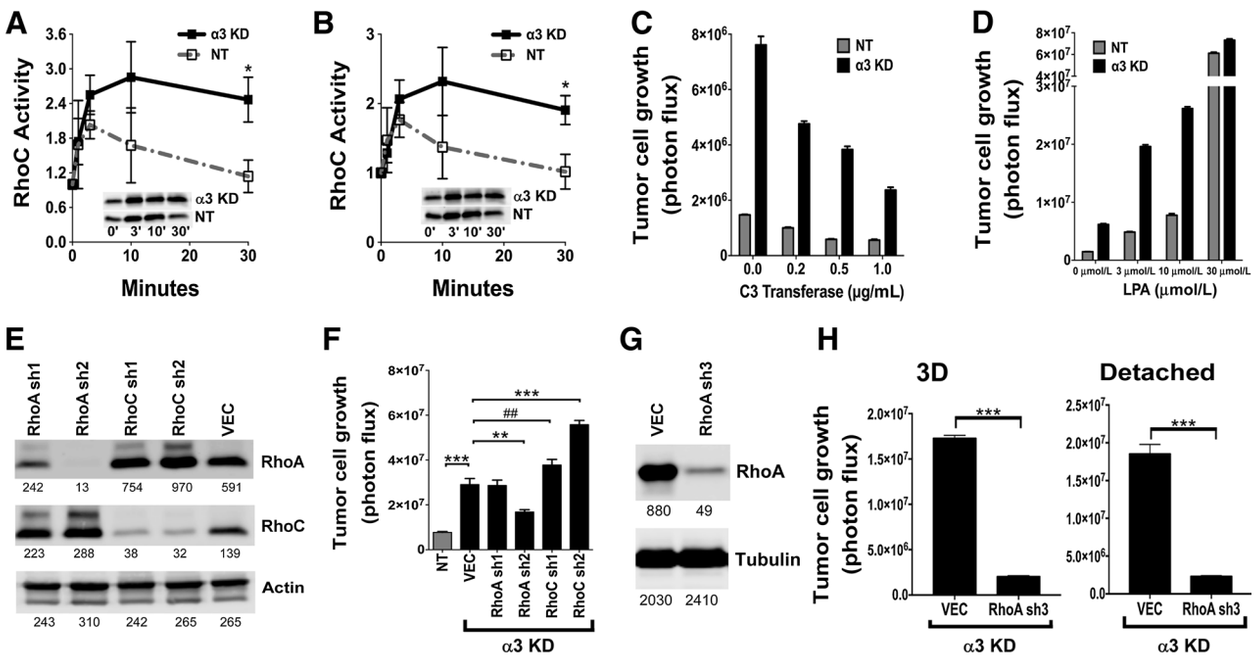


**Figure 3.**

The α3-KD cells display aberrant Rho GTPase signaling and depend on RhoA for increased growth in 3D. **A** and **B,** RhoA and RhoC activation elicited by 5 μmol/L LPA treatment was measured by GST-Rhotekin pulldown (*, $P = 0.0355$, unpaired $t$ test, RhoA; *, $P = 0.0492$, unpaired $t$ test, RhoC). Graphs show means ± SEM for four trials. Insets show representative blots of active RhoA and RhoC. **C,** treatment with C3-transferase drove down the 3D growth of the α3-KD cells in a dose-dependent manner. **D,** LPA promoted the 3D growth of the α3-KD cells and NT control cells. **E,** stable silencing of RhoA and RhoC in the α3-KD cells. Numbers indicate intensity units measured with a LiCOR blot imager. **F,** 3D growth assays comparing α3 integrin-expressing NT control cells to α3-KD cells harboring a nontar geting vector (VEC) or RhoA or RhoC shRNA constructs. Bars, ± SEM; $n = 6$. Differences in growth were analyzed by ANOVA with Holm–Sidak's multiple comparison test, ***, $P < 0.0001$; **, $P = 0.003$; ##, $P = 0.0041$; $\alpha = 0.05$. **G,** stable silencing of RhoA in α3-KD cells with a third shRNA; numbers indicate intensity units measured with a LiCOR blot imager. **H,** growth of α3-KD cells harboring a nontargeting vector (VEC) or the RhoA sh3 construct under 3D or detached conditions. Bars, ± SEM; $n = 6$. Differences in growth were analyzed by unpaired $t$ test, ***, $P < 0.0001$.

**Increased expression and nuclear localization of Hippo pathway targets YAP and TAZ in α3 integrin–depleted cells**

Several recent studies link Rho signaling and contractility to activation of proto-oncogenic transcriptional coactivators YAP1 and WWTR1/TAZ (11–13). In cells growing under detached conditions, YAP and TAZ were upregulated 2.5- to 3-fold in α3-KD cells compared with NT cells (Fig. 4A and B). Connective tissue growth factor (CTGF), a YAP/TAZ transcriptional target, was also upregulated in α3-KD cells (Fig. 4C). In addition, TAZ protein was upregulated in α3-KD DU-145 cells under detached conditions (Supplementary Fig. S5), consistent with their increased 3D growth (Supplementary Fig. S3D). In response to stimulation with 5 μmol/L LPA, α3-KD cells displayed a higher nuclear to cytoplasmic (N:C) ratio of TAZ and YAP than did NT cells (Fig. 4D–F), consistent with the prolonged activation of RhoA in α3-KD cells treated with this dose of LPA (Fig. 3A).

To examine the link between Rho signaling, YAP, and TAZ under conditions where α3-KD cells show increased growth compared with NT cells, we performed Rho pulldown assays on 3 biological replicates of cells growing under detached conditions. α3-KD cells showed increased RhoA activity compared with NT cells under these conditions (Supplementary Fig. S6A, S6B, and S6D), but not increased RhoC activity (Supplementary Fig. S6A, S6C, and S6E), consistent with the specific role of RhoA observed in Fig. 3. Moreover, YAP and TAZ were again upregulated in α3-KD cells compared with NT cells (Supplementary Fig. S6A, S6H, and S6I), further confirming results in Fig. 4A and B.

We used retroviral RNAi constructs to generate stable YAP or TAZ knockdown in α3-KD cells (Fig. 4G and Supplementary Fig. S7A and S7C). Interestingly, silencing TAZ, but not YAP, strongly suppressed the 3D growth of the cells (Fig. 4H and Supplementary Fig. S7B and S7D). YAP and TAZ are the targets of negative regulation by the Hippo pathway kinases, LATS1/2, but can also be activated by Rho signaling through LATS-independent mechanisms (11–13). Therefore, we silenced LATS1 in GS689.Li cells (Supplementary Fig. S8A). LATS1-silenced cells displayed a 7-fold increase in 3D growth compared with vector control or cells with inactive shRNAs (Supplementary Fig. S8B), phenocopying α3-KD cells. Conversely, force-expressing LATS1 in α3-KD cells partially reduced 3D growth (Supplementary Fig. S8C and S8D). An additional LATS1 shRNA produced moderate LATS1 knockdown and increased 3D growth compared with vector control or an inactive LATS1 shRNA (Supplementary Fig. S8E and S8F). These data are consistent with a role for LATS1 in α3-mediated growth suppression, but do not rule out LATS-independent mechanisms.

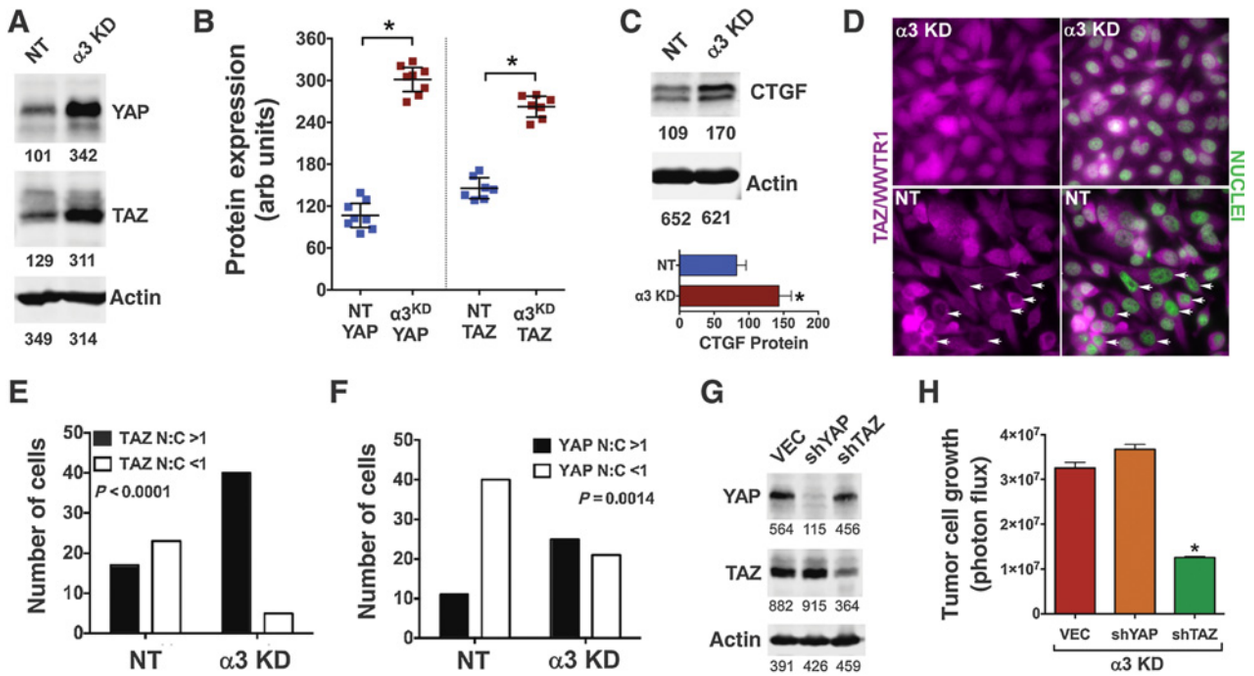


**Figure 4.**

The α3-KD cells show increased YAP and TAZ expression and depend on TAZ for increased 3D growth. **A,** immunoblot of YAP and TAZ in NT control and α3-KD cells growing under detached conditions. **B,** multiple independent experiments showed increased YAP and TAZ in α3-KD cells versus NT control cells. *, $P < 0.0001$, unpaired $t$ test. **C,** lysates of NT control and α3-KD cells growing under detached conditions were immunoblotted for CTGF. The graph shows mean CTGF levels in three trials after normalization to actin. **D,** serum-starved α3-KD or NT control cells were treated with 5 μmol/L LPA for 20 hours, then fixed and stained for TAZ (magenta), with nuclei counterstained with DAPI (green). Arrows, NT control cell nuclei with reduced or absent TAZ staining compared with adjacent cytoplasm. An identical experiment was performed for YAP (not shown). **E** and **F,** the proportions of cells with a nuclear:cytoplasmic (N:C) ratio of TAZ or YAP greater than or less than 1.0 were determined using ImageJ. A larger number of α3-KD cells displayed a nuclear:cytoplasmic ratio of TAZ and YAP>1 ($P < 0.0001$ or 0.0014, respectively, Fisher exact test, $n \geq 40$ cells). **G,** stable knockdown of YAP and TAZ in α3-KD cells. **H,** knockdown of TAZ but not YAP inhibited growth of the α3-KD cells on 3D collagen ($P < 0.0001$, ANOVA with Tukey post test; bars, ± SEM, $n = 6$). Numbers below immunoblots show intensity units measured with a LiCOR blot imager.

**The invasive growth of α3 integrin-depleted cells is linked to impaired Abl kinase signaling**

In neurons, α3β1 integrin activates the Arg/Abl2 tyrosine kinase, which in turn phosphorylates and activates a p190RhoGAP/p120RasGAP complex that inhibits Rho signaling (19). To investigate whether this pathway may be disrupted in our α3-KD cells growing in 3D collagen, we immunoprecipitated p190RhoGAP and blotted for (i) phosphotyrosine to detect activated p190, (ii) p120RasGAP to detect a p190/p120 complex, another readout for activated p190 (19), or (iii) total p190. Phospho-p190RhoGAP and p190-associated p120RasGAP were both reduced in α3-KD cells growing in 3D (Fig. 5A), consistent with the increased Rho activation in α3-KD cells. A similar result was obtained using cells growing in suspension (Supplementary Fig. S9A) and with an antibody that recognizes Abl family kinase phosphorylation sites on Crk and CrkL (Y221/Y207), another readout of Abl kinase activity (Supplementary Fig. S9B; ref. 22).

If an α3 integrin-Abl kinase pathway signals to suppress RhoA in prostate carcinoma cells, Abl kinase inhibitors might have paradoxical growth-promoting effects. Indeed, imatinib potently increased the 3D growth of NT cells by approximately 25-fold (Fig. 5B). For α3-KD cells, in which Abl kinase signaling may already be partially compromised (contributing to their ∼8-fold growth advantage over NT cells), imatinib only increased growth an additional approximately 3-fold (Fig. 5B). RhoA RNAi revealed that imatinib's pro-growth effects depend on the presence of RhoA (Fig. 5C).

We next depleted Arg by RNAi. Silencing Arg by 75% (sh1 construct) or 99% (sh2 construct) dramatically increased the 3D growth of the cells, with stronger silencing leading to a greater growth increase (Fig. 5D). Silencing Abl1 kinase also increased 3D growth, indicating that Abl1 and Arg cooperate to limit 3D growth (Fig. 5E). To investigate the effects of stimulating Abl kinase activity, we treated cells with the Abl kinase activator, DPH (23). A dose of 3 μmol/L, near the reported cellular $EC_{50}$ (23), abolished the growth of α3-KD cells in 3D (Fig. 5F), but had no effect on their growth under standard culture conditions (Fig. 5G).

The above experiments provided mechanistic insight into the increased growth of α3-depleted cells, but our *in vivo* assays suggested that more rapid growth of α3-KD tumors was not sufficient to explain their increased dissemination. Using time-lapse microscopy, we found that α3-KD cells migrate significantly faster than NT cells (Fig. 6A and B); α3-KD cells also showed increased invasion towards LPA in a transwell assay (Fig. 6C and D). Imatinib increased the mean migration speed of NT cells up to that of α3-KD cells (Fig. 6E). Conversely, DPH potently suppressed cell motility (Fig. 6F). In aggregate, our data support a model in which α3 integrin signals through Abl kinases to activate p190RhoGAP, suppress RhoA activity, and support Hippo pathway function. Upon loss of α3 integrin, this pathway is disrupted,

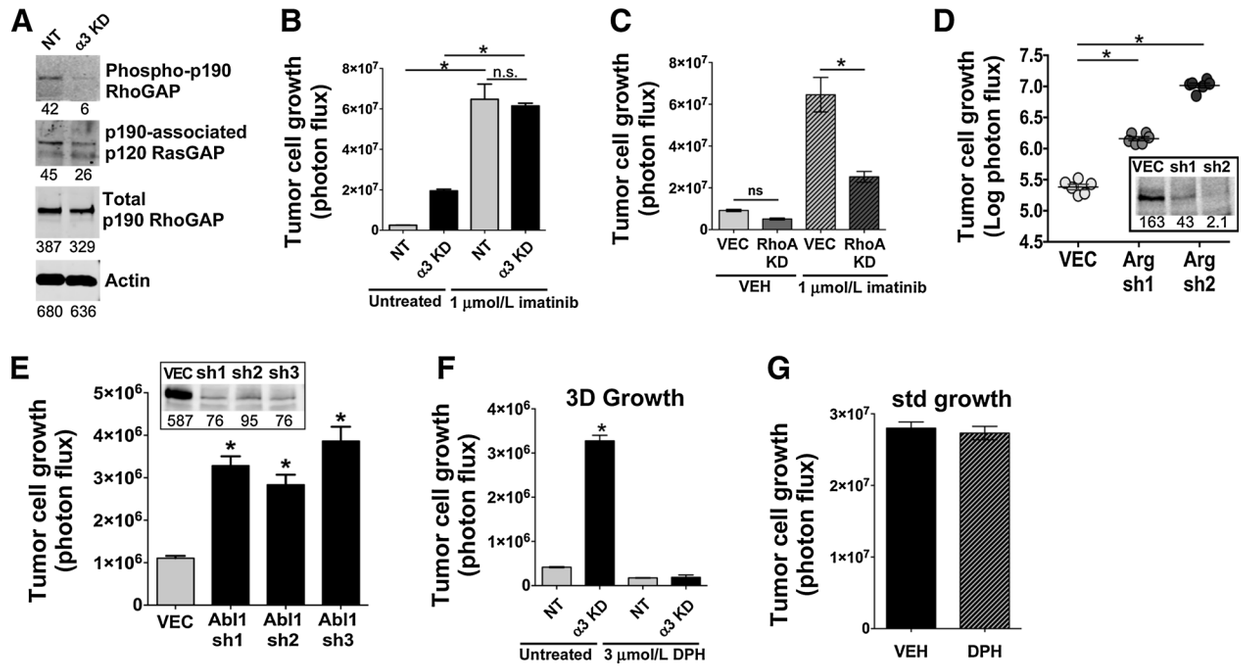


**Figure 5.**

Increased 3D growth of α3-KD cells is linked to impaired Abl kinase signaling. **A,** the Arg/Abl2 substrate, p190RhoGAP, was immunoprecipitated from lysates of cells growing on 3D collagen in the presence of 5 μmol/L LPA. p190RhoGAP immunoprecipitations were blotted for phosphotyrosine, p120RasGAP, or total p190RhoGAP. **B,** imatinib increased the growth of NT control cells by approximately 25-fold and the growth of α3-KD cells by approximately 3-fold; *, $P < 0.0001$, ANOVA with Tukey post test. **C,** a RhoA knockdown but not a nontargeting control vector (VEC) blocked the increased 3D growth of NT control cells caused by imatinib; *, $P < 0.0001$, ANOVA with Tukey post test. **D,** knockdown of Arg/Abl2 dramatically increased 3D growth of GS689.Li cells; *, $P < 0.0001$, ANOVA with Tukey post test. Inset, immunoblotting of Arg in cells harboring a nontargeting control vector (VEC) or Arg sh1 or sh2 constructs. **E,** knockdown of Abl1 significantly increased 3D growth of GS689.Li cells; *, $P < 0.0001$, ANOVA with Tukey post test. Inset, immunoblotting of Abl in cells with nontargeting control vector (VEC) or the three shRNA constructs. **F,** Abl kinase activator, DPH, abolished the increased 3D growth of the α3-KD cells. *, $P < 0.0001$, ANOVA with Tukey post test. **G,** DPH had no effect on α3-KD tumor cell growth under standard tissue culture conditions.

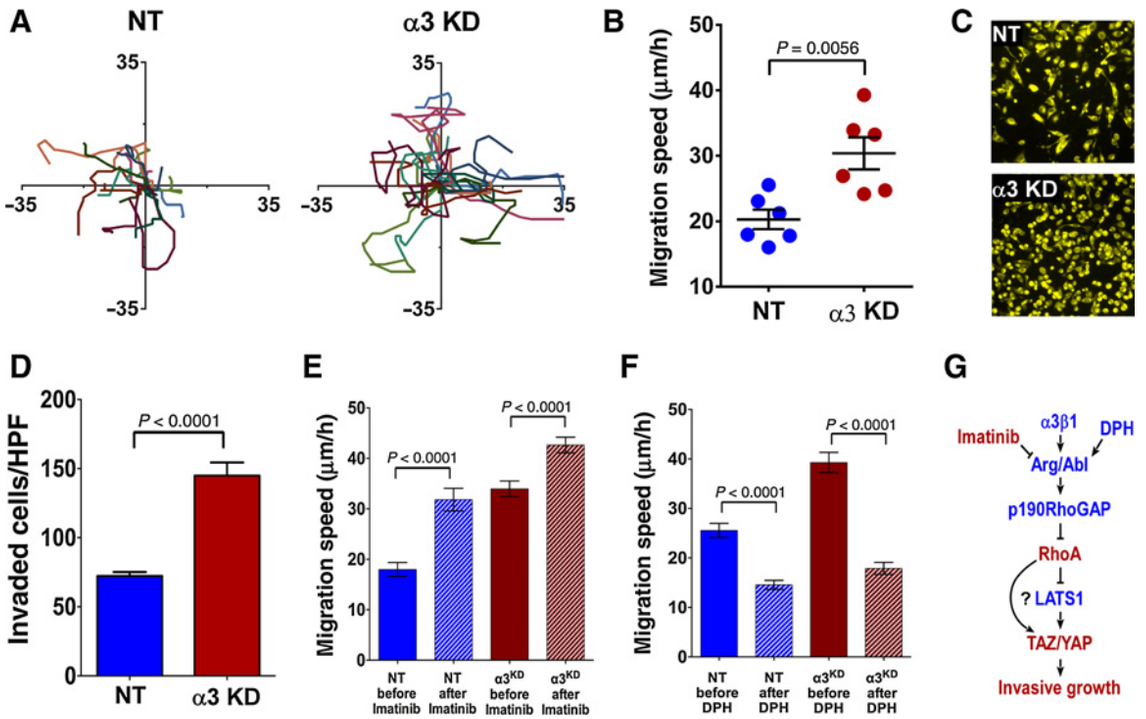


**Figure 6.**

α3 integrin and Abl kinase activity restrain migration and invasion. **A,** cell motility tracks for NT control and α3-KD cells migrating on collagen I monitored by time-lapse microscopy; $n = 20$ tracks for each cell type. **B,** migration speed for NT control and α3-KD cells on collagen I for six independent trials; $n \geq 50$ cells of each type per experiment; $P = 0.0056$, unpaired $t$ test. **C,** high powered fields of migrated cells in a transwell invasion assay with NT control and α3-KD cells migrating towards 5 μmol/L LPA in the bottom chamber. **D,** quantification of invasion assay showing mean ± SEM of invaded cells; $n = 4$ fields in each of 3 wells/cell type; $P < 0.0001$ unpaired $t$ test. **E,** time-lapse microscopy of NT control cells and α3-KD cells before and after 5 μmol/L imatinib addition; $P < 0.0001$, paired $t$ test. **F,** time-lapse microscopy of NT control and α3-KD cells before and after addition of 3 μmol/L DPH. $P < 0.0001$, paired $t$ test. **G,** working model. Suppressors of invasive growth are shown in blue and promoters in red.

resulting in increased RhoA activation, and increased TAZ/YAP activity driving invasive growth (Fig. 6G). TAZ/YAP activation by RhoA may involve both LATS1-dependent and -independent mechanisms.

A parallel mechanism for the increased 3D growth of α3-KD cells could involve altered signaling through FAK, a major integrin effector. Indeed, FAK activation was increased in α3-KD cells compared with NT cells growing under detached conditions (Supplementary Fig. S10A). However, the selective FAK inhibitor PF-573228 failed to block 3D growth of either α3-KD or NT cells (Supplementary Fig. S10B). Therefore, we currently favor an α3-Abl kinase-Hippo pathway signaling axis as the explanation for the increased growth of α3-depleted prostate carcinoma cells.

### Loss of α3 integrin and increased nuclear TAZ and YAP in human prostate carcinoma

Our data suggested that loss of α3 integrin expression and altered TAZ and YAP activity may cooccur in prostate cancer. Therefore, we examined α3 integrin, TAZ, and YAP expression on adjacent sections of a human prostate cancer tissue microarray. We observed frequent downregulation of α3 integrin in prostate cancer compared with the strong basolateral staining found in benign glands (Fig. 7A and B). TAZ and YAP nuclear staining was observed in the proliferative basal cell layer of benign prostate glands, as reported previously (24), but TAZ was mainly absent from luminal cells of benign glands, and YAP localization was cytoplasmic rather than nuclear in luminal cells (Fig. 7C–F). In contrast, TAZ and YAP nuclear staining were prominent in prostate carcinoma (Fig. 7C–F). We quantified staining using a quartile scoring system (Supplementary Fig. S11; see Materials and Methods). Each core was assigned a primary and secondary score, which were summed, similar to the Gleason scoring system. These analyses confirmed that α3 integrin was significantly downregulated and nuclear TAZ and YAP were significantly upregulated in cancerous glands, compared with differentiated luminal cells of benign prostate epithelia (Fig. 7G).

## Discussion

While evidence of Hippo pathway disruptions in prostate cancer continues to mount (25–27), little is known about the cell surface inputs that regulate the pathway. We now provide evidence that a cell surface receptor, α3β1 integrin, signals through Abl kinases to restrain Rho activity, support Hippo pathway function, and inhibit metastasis. Our study contributes to an emerging theme of α3β1 integrin as a moderator of Rho activity. Depleting α3 integrin activates RhoA in breast cancer cells (28) and loss of the α3 partner, tetraspanin CD151, drives

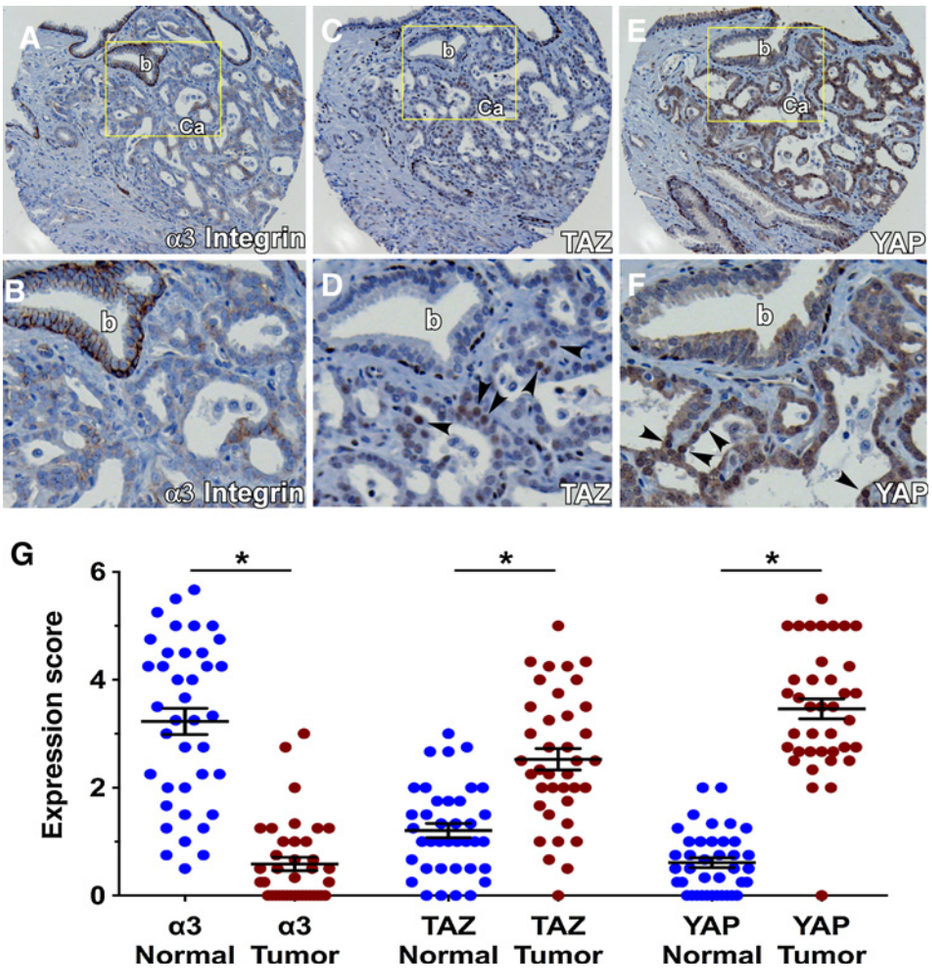


**Figure 7.**
Loss of α3 integrin and increased nuclear TAZ and YAP in human prostate cancer specimens. Immunohistochemical staining of α3 integrin (**A** and **B**), TAZ (**C** and **D**), and YAP (**E** and **F**) on adjacent sections of a prostate cancer tissue microarray. **B**, **D**, and **F,** enlarged views of the indicated fields in **A**, **C**, and **E** (b, benign gland; Ca, prostate carcinoma). Arrowheads, nuclear TAZ and YAP staining in prostate carcinoma. **G,** mean staining scores for α3 integrin, TAZ, and YAP on a 40 case microarray of human prostate cancer and matched normal tissues. Each case was represented by four cores of cancer and four cores of normal tissue. Each point represents the average score for each patient sample, across the four cores. The expression of α3 integrin was reduced, while nuclear expression of TAZ and YAP was increased in tumor versus normal glands; *, $P < 0.0001$, paired *t* test. For scoring TAZ and YAP in normal glands, only luminal cells were considered.

Rho-dependent collective invasion (29). Conditional deletion of α3 integrin in mice deregulated Rho activity, disrupting the contractility–relaxation cycle of mammary myoepithelial cells (18) and the morphology of hippocampal neurons (19). Interestingly, we found that the increased 3D growth of α3-KD cells depends specifically on RhoA rather than RhoC. The basis for this specificity requires further investigation, but a potential clue comes from ovarian cancer cells, where RhoA but not RhoC signaled to promote YAP activation (30). RhoC might still contribute to the enhanced migration, invasion, and metastasis of α3 integrin-deficient prostate cancer cells, as RhoC can promote breast cancer or melanoma metastasis without influencing primary tumor growth (31, 32).

Deregulated Abl kinase activity can drive malignant progression (33–35), but Abl kinase signaling can also suppress tumor growth in some contexts (33, 36). In MDA-MB-231 breast cancer xenografts, the Arg knockdown dramatically potentiated primary tumor growth and lung metastatic colonization after tail vein inoculation, but suppressed spontaneous metastasis from the mammary fat pad (33). However, loss of Arg was accompanied by downregulation of Rho GTPase expression (33), which we did not observe in our α3-KD cells, and which thus may help to explain context-specific differences between the breast and prostate cancer models.

Context-specific, pro-, and anti-tumor functions have also been reported for α3 integrin (8, 10, 37–40). Factors that influence whether α3β1 promotes or restrains tumor progression may include (i) whether the tumor secretes an α3β1 integrin ligand (38), (ii) the stage at which tumor progression is being modeled (39), (iii) the role of α3 integrin in controlling mRNA splicing (41), and (iv) the downstream signaling pathways driving malignant progression. For example, α3β1 promotes Rac activation (42), even as it limits Rho activity, and is required for Rac-driven mammary tumors (40), even as it restrains Rho-driven prostate carcinomas, as we show here.

In contrast to our results, imatinib in combination with paclitaxel was reported to inhibit the growth of a PC-3 prostate cancer subline in an intratibial model of tumor growth (43). In this preclinical model, imatinib was intended to target the PDGF receptor on tumor-associated endothelial cells and bone-adjacent tumor cells. Imatinib treatment inhibited proliferation and increased apoptosis of tumor cells growing in bone, but not cells invading into adjacent tissue (43). Thus, the effect of imatinib on prostate cancer growth *in vivo* is context-dependent, and the potential for endogenous Abl kinases to suppress the growth of PDGFR-independent tumor cells might help to explain the failure of the Abl kinase inhibitor imatinib in prostate cancer clinical trials, where imatinib treatment was associated with lower

probability of PSA decline, and shorter progression-free and overall survival (44).

There is growing recognition that Hippo pathway disruptions promote not only tumorigenesis, but also progression and metastasis (27, 45–47). Intriguingly, TAZ but not YAP was required for the increased 3D growth of α3-KD cells, reminiscent of the dominant role of TAZ in promoting expansion of human embryonic stem cells (48). Nuclear localized YAP promotes tumor growth, but cytoplasmic YAP can suppress proliferation (49), which might help to explain why we observed no net effect on tumor cell growth upon YAP depletion. However, YAP might still contribute to increased invasion and metastasis (45). Therefore, further studies are required to determine the relative contributions of TAZ and YAP to different stages of prostate cancer progression.

The working hypothesis supported by our data provides several clear predictions and potential therapeutic opportunities based on the context of α3 integrin expression. First, while Abl kinases can function as oncogenes in some contexts, our data predict that they could function as tumor suppressors in others, such as α3 integrin-deficient prostate cancers. If substantiated, this could lead to novel strategies involving the use of small-molecule activators of Abl kinases (23) in carefully selected circumstances, and better informed use of multi-tyrosine kinase inhibitors that cross-inhibit Abl. A second prediction of our hypothesis is that, when present, the antitumor activity of Abl kinases stems from signaling to suppress Rho activity and thereby inhibit TAZ/YAP. This would provide a key mechanistic insight to explain how Abl inhibitors such as imatinib can sometimes paradoxically fuel cancer proliferation. Finally, our model predicts that the increased progression and metastasis of α3-depleted prostate cancer cells requires TAZ (and potentially YAP), advancing α3-deficient prostate cancers as potential candidates for treatment with Hippo-directed therapies under preclinical development (13).

## Disclosure of Potential Conflicts of Interest

J.A. Brown reports receiving a commercial research grant from Myriad. No potential conflicts of interest were disclosed by the other authors.

## Authors' Contributions

**Conception and design:** A. Varzavand, K.N. Gibson-Corley, M.D. Henry, C.S. Stipp

**Development of methodology:** A. Varzavand, M.D. Henry, C.S. Stipp

**Acquisition of data (provided animals, acquired and managed patients, provided facilities, etc.):** W. Hacker, D. Ma, K.N. Gibson-Corley, M. Hawayek, J.A. Brown, M.D. Henry, C.S. Stipp

**Analysis and interpretation of data (e.g., statistical analysis, biostatistics, computational analysis):** A. Varzavand, W. Hacker, D. Ma, K.N. Gibson-Corley, M. Hawayek, O.J. Tayh, C.S. Stipp

**Writing, review, and/or revision of the manuscript:** A. Varzavand, K.N. Gibson-Corley, J.A. Brown, M.D. Henry, C.S. Stipp

**Administrative, technical, or material support (i.e., reporting or organizing data, constructing databases):** A. Varzavand

**Study supervision:** M.D. Henry, C.S. Stipp

## Acknowledgments

Dr. Brown is the current University of Iowa Andersen-Hebbeln Professor in Prostate Cancer Research. This endowed professorship provided financial support related to this research effort.

## Grant Support

Core facilities used in these studies were supported by NIH grant P30 CA086862. This work was supported by NIH R01 grants CA13664 (C.S. Stipp) and CA130916 (M.D. Henry), and the Department of Defense Prostate Cancer Research Program Award #W81XWH-14-2-0182, W81XWH-14-2-0183, W81XWH-14-2-0185, W81XWH-14-2-0186, and W81XWH-15-2-0062 to the Prostate Cancer Biorepository Network (PCBN). The Cancer Genes and Pathways program at the UI Holden Comprehensive Cancer Center provided financial support for the publication of this study.

The costs of publication of this article were defrayed in part by the payment of page charges. This article must therefore be hereby marked *advertisement* in accordance with 18 U.S.C. Section 1734 solely to indicate this fact.

Received June 3, 2016; revised August 22, 2016; accepted September 4, 2016; published OnlineFirst September 28, 2016.

## References

1. Goel HL, Alam N, Johnson INS, Languino LR. Integrin signaling aberrations in prostate cancer. Am J Transl Res 2009;1:211–20.
2. Sroka IC, Anderson TA, McDaniel KM, Nagle RB, Gretzer MB, Cress AE. The laminin binding integrin alpha6beta1 in prostate cancer perineural invasion. J Cell Physiol 2010;224:283–8.
3. Alva A, Slovin S, Daignault S, Carducci M, Dipaola R, Pienta K, et al. Phase II study of cilengitide (EMD 121974, NSC 707544) in patients with non-metastatic castration resistant prostate cancer, NCI-6735. A study by the DOD/PCF prostate cancer clinical trials consortium. Invest New Drugs 2012;30:749–57.
4. Bradley DA, Daignault S, Ryan CJ, Dipaola RS, Cooney KA, Smith DC, et al. Cilengitide (EMD 121974, NSC 707544) in asymptomatic metastatic castration resistant prostate cancer patients: a randomized phase II trial by the prostate cancer clinical trials consortium. Invest New Drugs 2011;29:1432–40.
5. Heidenreich A, Rawal SK, Szkarlat K, Bogdanova N, Dirix L, Stenzl A, et al. A randomized, double-blind, multicenter, phase 2 study of a human monoclonal antibody to human $\alpha v$ integrins (intetumumab) in combination with docetaxel and prednisone for the first-line treatment of patients with metastatic castration-resistant prostate cancer. Ann Oncol 2013;24:329–36.
6. Giancotti FG, Ruoslahti E. Elevated levels of the alpha 5 beta 1 fibronectin receptor suppress the transformed phenotype of Chinese hamster ovary cells. Cell 1990;60:849–59.
7. Zutter MM, Santoro SA, Staatz WD, Tsung YL. Re-expression of the alpha 2 beta 1 integrin abrogates the malignant phenotype of breast carcinoma cells. Proc Natl Acad Sci U S A 1995;92:7411–5.
8. Weitzman JB, Hemler ME, Brodt P. Reduction of tumorigenicity by alpha 3 integrin in a rhabdomyosarcoma cell line. Cell Adhes Commun 1996;4:41–52.
9. Schmelz M, Cress AE, Scott KM, Bürger F, Cui H, Sallam K, et al. Different phenotypes in human prostate cancer: alpha6 or alpha3 integrin in cell-extracellular adhesion sites. Neoplasia 2002;4:243–54.
10. Varzavand A, Drake JM, Svensson RU, Herndon ME, Zhou B, Henry MD, et al. Integrin $\alpha 3\beta 1$ regulates tumor cell responses to stromal cells and can function to suppress prostate cancer metastatic colonization. Clin Exp Metastasis 2013;30:541–52.
11. Yu F-X, Zhao B, Guan K-L. Hippo pathway in organ size control, tissue homeostasis, and cancer. Cell 2015;163:811–28.
12. Piccolo S, Dupont S, Cordenonsi M. The biology of YAP/TAZ: Hippo signaling and beyond. Physiol Rev 2014;94:1287–312.
13. Johnson R, Halder G. The two faces of Hippo: targeting the Hippo pathway for regenerative medicine and cancer treatment. Nat Rev Drug Discov 2014;13:63–79.
14. Drake JM, Strohbehn G, Bair TB, Moreland JG, Henry MD. ZEB1 enhances transendothelial migration and represses the epithelial phenotype of prostate cancer cells. Mol Biol Cell 2009;20:2207–17.
15. Zevian S, Winterwood NE, Stipp CS. Structure-function analysis of tetraspanin CD151 reveals distinct requirements for tumor cell behaviors mediated by $\alpha 3\beta 1$ versus $\alpha 6\beta 4$ integrin. J Biol Chem 2011;286:7496–506.
16. Meijering E, Dzyubachyk O, Smal I. Methods for cell and particle tracking. Meth Enzymol 2012;504:183–200.

17. Johnson JL, Winterwood N, DeMali KA, Stipp CS. Tetraspanin CD151 regulates RhoA activation and the dynamic stability of carcinoma cell-cell contacts. J Cell Sci 2009;122:2263–73.
18. Raymond K, Cagnet S, Kreft M, Janssen H, Sonnenberg A, Glukhova MA. Control of mammary myoepithelial cell contractile function by $\alpha 3\beta 1$ integrin signalling. EMBO J 2011;30:1896–906.
19. Kerrisk ME, Greer CA, Koleske AJ. Integrin $\alpha 3$ is required for late postnatal stability of dendrite arbors, dendritic spines and synapses, and mouse behavior. J Neurosci 2013;33:6742–52.
20. Schackmann RCJ, van Amersfoort M, Haarhuis JHI, Vlug EJ, Halim VA, Roodhart JML, et al. Cytosolic p120-catenin regulates growth of metastatic lobular carcinoma through Rock1-mediated anoikis resistance. J Clin Invest 2011;121:3176–88.
21. Giang Ho TT, Stultiens A, Dubail J, Lapière CM, Nusgens BV, Colige AC, et al. RhoGDIα-dependent balance between RhoA and RhoC is a key regulator of cancer cell tumorigenesis. Mol Biol Cell 2011;22:3263–75.
22. Ganguly SS, Fiore LS, Sims JT, Friend JW, Srinivasan D, Thacker MA, et al. c-Abl and Arg are activated in human primary melanomas, promote melanoma cell invasion via distinct pathways, and drive metastatic progression. Oncogene 2012;31:1804–16.
23. Yang J, Campobasso N, Biju MP, Fisher K, Pan X-Q, Cottom J, et al. Discovery and characterization of a cell-permeable, small-molecule c-Abl kinase activator that binds to the myristoyl binding site. Chem Biol 2011;18:177–86.
24. Zhao B, Wei X, Li W, Udan RS, Yang Q, Kim J, et al. Inactivation of YAP oncoprotein by the Hippo pathway is involved in cell contact inhibition and tissue growth control. Genes Dev 2007;21:2747–61.
25. Nguyen LT, Tretiakova MS, Silvis MR, Lucas J, Klezovitch O, Coleman I, et al. ERG activates the YAP1 transcriptional program and induces the development of age-related prostate tumors. Cancer Cell 2015; 27:797–808.
26. Zhang L, Yang S, Chen X, Stauffer S, Yu F, Lele SM, et al. The hippo pathway effector YAP regulates motility, invasion, and castration-resistant growth of prostate cancer cells. Mol Cell Biol 2015;35:1350–62.
27. Zhao B, Li L, Wang L, Wang C-Y, Yu J, Guan K-L. Cell detachment activates the Hippo pathway via cytoskeleton reorganization to induce anoikis. Genes Dev 2012;26:54–68.
28. Novitskaya V, Romanska H, Kordek R, Potemski P, Kusin´ska R, Parsons M, et al. Integrin $\alpha 3\beta 1$-CD151 complex regulates dimerization of ErbB2 via RhoA. Oncogene 2014;33:2779–89.
29. Zevian SC, Johnson JL, Winterwood NE, Walters KS, Herndon ME, Henry MD, et al. CD151 promotes $\alpha 3\beta 1$ integrin-dependent organization of carcinoma cell junctions and restrains collective cell invasion. Cancer Biol Ther 2015;16:1626–40.
30. Cai H, Xu Y. The role of LPA and YAP signaling in long-term migration of human ovarian cancer cells. Cell Commun Signal 2013;11:31.
31. Hakem A, Sanchez-Sweatman O, You-Ten A, Duncan G, Wakeham A, Khokha R, et al. RhoC is dispensable for embryogenesis and tumor initiation but essential for metastasis. Genes Dev 2005;19:1974–9.
32. Clark EA, Golub TR, Lander ES, Hynes RO. Genomic analysis of metastasis reveals an essential role for RhoC. Nature 2000;406:532–5.
33. Gil-Henn H, Patsialou A, Wang Y, Warren MS, Condeelis JS, Koleske AJ. Arg/Abl2 promotes invasion and attenuates proliferation of breast cancer *in vivo*. Oncogene 2013;32:2622–30.
34. Greuber EK, Smith-Pearson P, Wang J, Pendergast AM. Role of ABL family kinases in cancer: from leukaemia to solid tumours. Nat Rev Cancer 2013;13:559–71.
35. Wang J, Rouse C, Jasper JS, Pendergast AM. ABL kinases promote breast cancer osteolytic metastasis by modulating tumor-bone interactions through TAZ and STAT5 signaling. Sci Signal 2016;9:ra12–2.
36. Allington TM, Galliher-Beckley AJ, Schiemann WP. Activated Abl kinase inhibits oncogenic transforming growth factor-beta signaling and tumorigenesis in mammary tumors. FASEB J 2009;23:4231–43.
37. Mitchell K, Svenson KB, Longmate WM, Gkirtzimanaki K, Sadej R, Wang X, et al. Suppression of integrin alpha3beta1 in breast cancer cells reduces cyclooxygenase-2 gene expression and inhibits tumorigenesis, invasion, and cross-talk to endothelial cells. Cancer Res 2010;70:6359–67.
38. Zhou B, Gibson-Corley KN, Herndon ME, Sun Y, Gustafson-Wagner E, Teoh-Fitzgerald M, et al. Integrin $\alpha 3\beta 1$ can function to promote spontaneous metastasis and lung colonization of invasive breast carcinoma. Mol Cancer Res 2014;12:143–54.
39. Sachs N, Secades P, van Hulst L, Kreft M, Song J-Y, Sonnenberg A. Loss of integrin $\alpha 3$ prevents skin tumor formation by promoting epidermal turnover and depletion of slow-cycling cells. Proc Natl Acad Sci U S A 2012;109:21468–73.
40. Cagnet S, Faraldo MM, Kreft M, Sonnenberg A, Raymond K, Glukhova MA. Signaling events mediated by $\alpha 3\beta 1$ integrin are essential for mammary tumorigenesis. Oncogene 2014;33:4286–95.
41. Subbaram S, Lyons SP, Svenson KB, Hammond SL, McCabe LG, Chittur SV, et al. Integrin $\alpha 3\beta 1$ controls mRNA splicing that determines Cox-2 mRNA stability in breast cancer cells. J Cell Sci 2014;127:1179–89.
42. Choma DP, Pumiglia K, Dipersio CM. Integrin alpha3beta1 directs the stabilization of a polarized lamellipodium in epithelial cells through activation of Rac1. J Cell Sci 2004;117:3947–59.
43. Uehara H, Kim S-J, Karashima T, Shepherd DL, Fan D, Tsan R, et al. Effects of blocking platelet-derived growth factor-receptor signaling in a mouse model of experimental prostate cancer bone metastases. J Natl Cancer Inst 2003;95:458–70.
44. Rosenberg A, Mathew P. Imatinib and prostate cancer: lessons learned from targeting the platelet-derived growth factor receptor. Expert Opin Investig Drugs 2013;22:787–94.
45. Lamar JM, Stern P, Liu H, Schindler JW, Jiang Z-G, Hynes RO. The Hippo pathway target, YAP, promotes metastasis through its TEAD-interaction domain. Proc Natl Acad Sci U S A 2012;109:E2441–50.
46. Chen D, Sun Y, Wei Y, Zhang P, Rezaeian AH, Teruya-Feldstein J, et al. LIFR is a breast cancer metastasis suppressor upstream of the Hippo-YAP pathway and a prognostic marker. Nat Med 2012;18:1511–7.
47. Bartucci M, Dattilo R, Moriconi C, Pagliuca A, Mottolese M, Federici G, et al. TAZ is required for metastatic activity and chemoresistance of breast cancer stem cells. Oncogene 2015;34:681–90.
48. Ohgushi M, Minaguchi M, Sasai Y. Rho-signaling-directed YAP/TAZ activity underlies the long-term survival and expansion of human embryonic stem cells. Cell Stem Cell 2015;17:448–61.
49. Barry ER, Morikawa T, Butler BL, Shrestha K, la Rosa de R, Yan KS, et al. Restriction of intestinal stem cell expansion and the regenerative response by YAP. Nature 2013;493:106–10.